

## Controlling the Dzyaloshinskii-Moriya interaction to alter the chiral link between structure and magnetism for $\text{Fe}_{1-x}\text{Co}_x\text{Si}$

S.-A. Siegfried,<sup>1</sup> E. V. Altyntbaev,<sup>2,3</sup> N. M. Chubova,<sup>2</sup> V. Dyadkin,<sup>2,4</sup> D. Chernyshov,<sup>4</sup> E. V. Moskvina,<sup>2,3</sup> D. Menzel,<sup>5</sup> A. Heinemann,<sup>1</sup> A. Schreyer,<sup>1</sup> and S. V. Grigoriev<sup>2,3</sup>

<sup>1</sup>*Helmholtz Zentrum Geesthacht, Geesthacht, 21502, Germany*

<sup>2</sup>*Petersburg Nuclear Physics Institute, Gatchina, St. Petersburg, 188300, Russia*

<sup>3</sup>*Saint-Petersburg State University, Ulyanovskaya 1, St. Petersburg, 198504, Russia*

<sup>4</sup>*Swiss-Norwegian Beamlines at the European Synchrotron Radiation Facility, Grenoble, 38000, France*

<sup>5</sup>*Institut für Physik der Kondensierten Materie, TU Braunschweig, 38106 Braunschweig, Germany*

(Received 16 February 2015; revised manuscript received 1 May 2015; published 14 May 2015)

Monosilicides of 3d metals frequently show a chiral magnetic ordering with the absolute configuration defined by the chirality of the crystal structure and the sign of the Dzyaloshinskii-Moriya interaction (DMI). Structural and magnetic chiralities are probed here for  $\text{Fe}_{1-x}\text{Co}_x\text{Si}$  series and their mutual relationship is found to be dependent on the chemical composition. The chirality of crystal structure was previously shown to be governed by crystal growth, and the value of the DMI is nearly the same for all monosilicides of Fe, Co, and Mn. Our findings indicate that the sign of the DMI in  $\text{Fe}_{1-x}\text{Co}_x\text{Si}$  is controlled by the Co composition  $x$ . We have been able to directly measure the change of the link between structure and magnetism in this helimagnetic B20 alloy.

DOI: [10.1103/PhysRevB.91.184406](https://doi.org/10.1103/PhysRevB.91.184406)

PACS number(s): 75.25.-j, 61.05.fg

Scattering of polarized neutrons on chiral magnetic structures allows one to determine the absolute magnetic configuration, and thus left- and right-handed helices can be easily distinguished [1]. On the other hand, by knowing the magnetic configuration, one can analyze the polarization of a scattering beam [2]. Similar effects could also help to manipulate spin polarization of an electron current, providing that the electrons interact with the known chiral magnetic structure.

The ability to manipulate the electron spin is a necessary component for the spintronics [3], and thus magnetic chiral organic molecules [4] or large-scale magnetic structures have been proposed as such tools [5]. However, the question of how to get the magnetic structure of a necessary chirality for spintronics applications is still open. Here we address the question for the case of  $\text{Fe}_{1-x}\text{Co}_x\text{Si}$  solid solutions which, for certain compositions, show chiral (spiral) magnetic ordering [6–8].

The structural chirality in monosilicides of 3d metals is solely controlled by crystal growth [9]. A link between the structural and magnetic chiralities is provided by the Dzyaloshinskii-Moriya interaction (DMI) and has been experimentally proved for many monosilicides of 3d metals [9–12]. The strength of the DMI defines the pitch of the magnetic spiral while the sign of the DMI sets a relationship between structural and magnetic chiralities to be the same or opposite [7,13].

For powder samples of  $\text{Mn}_{1-x}\text{Fe}_x\text{Ge}$  [12,14] and  $\text{Fe}_{1-x}\text{Co}_x\text{Ge}$  [15] it was shown that the spiral wave vector  $k = 2\pi/d$ , where  $d$  is the spiral period, goes to zero value at a certain composition. The monotonic behavior of the wave vector indicates that the DMI goes to zero at the very same composition and, therefore, should change its sign as a function of  $x$  [12,15].

Here we further exploit the idea to control the DMI sign for the monosilicide series  $\text{Fe}_{1-x}\text{Co}_x\text{Si}$ . At variance with the germanides, the silicides can be grown as single crystals with controlled structural chirality [9]. A large size of crystals also makes possible a combined determination of the structural  $\Gamma_c$

and magnetic  $\gamma_m$  chiralities by resonant x-ray diffraction and polarized neutron scattering, correspondingly. Here and below chiralities are defined according to Ref. [13]. Taken together, the two experimental probes allow us to follow  $\Gamma_c \times \gamma_m$  as a function of composition  $x$ . Thus, the sign of the DMI term in the Hamiltonian of Ref. [7,8] can be experimentally probed via the product  $\Gamma_c \times \gamma_m$ , allowing us to directly observe the flip of the link of the structural and magnetic chirality with the concentration  $x$ .

Single crystals of  $\text{Fe}_{1-x}\text{Co}_x\text{Si}$  were grown using the Czochralski technique for the following concentrations:  $x = 0.5, 0.6, 0.65, 0.7, 0.8$ . The same structural chirality of all grown crystals was provided by a consequent use of every grown crystal as the seed for the next one. As was shown before, this technique gives almost 100% control of the structural chirality [9]. The absolute crystal structure can be established by the x-ray single-crystal diffraction data, and resonant contribution enables us to observe violation of the Friedel law. More details can be found in Refs. [16–18].

Single-crystal Bragg diffraction data were collected at the room temperature using the PILATUS@SNBL diffractometer at the BM01A end station of the Swiss-Norwegian Beamlines at the ESRF (Grenoble, France); the wavelength of the synchrotron radiation was set to 0.70135 Å. The data were collected with a single  $\phi$  scan with angular step of 0.1° in a shutter-free mode with the Pilatus2M detector. The raw data were preprocessed with SNBL TOOLBOX, the integral intensities were extracted from the frames with the CRYSLIS PRO software [19], and the crystal structure was solved with SHELXS and refined with SHELXI [20]. Crystals with an average size of about 100 microns were cut from large single crystals. The diffraction data are summarized in Table I.

The data are of good quality and agreement with the structural P2<sub>1</sub>3 model is high as can be seen from R factors. The unit cell dimensions follow the Vegard law but the atomic positions stay nearly the same as a function of composition; the absolute structure is defined according to their values.

TABLE I. Diffraction data for  $\text{Fe}_{1-x}\text{Co}_x\text{Si}$  with  $x = 0.6, 0.65, 0.7, 0.8$ .

$x$	$R_i$	$R_1$	$R_w$	$x_{\text{Me}}$	$x_{\text{Si}}$	Flack
0.6	0.025	0.0295	0.0811	0.86000(2)	0.1579(5)	0.02(5)
0.65	0.017	0.0110	0.0290	0.85989(9)	0.1572(2)	0.01(4)
0.7	0.016	0.0299	0.0665	0.85968(19)	0.1575(4)	0.10(7)
0.8	0.049	0.0193	0.0420	0.85882(13)	0.1571(3)	-0.01(7)

Thus, in agreement with definitions given in Refs. [16,21], the chirality  $\Gamma_c$  of structure with  $x_{\text{Me}} \approx 0.86$  is set to +1. The Flack parameter, which is a measure of presence of domains with the opposite chirality, is zero within  $1 \div 2$  standard deviations; the results confirm the same absolute structure (i.e., the same structural chirality) for all the tested crystals, as expected from the crystal growth procedure.

$\text{Fe}_{1-x}\text{Co}_x\text{Si}$  compounds are magnetically ordered in the concentration range  $0.05 \leq x \leq 0.8$  [22,23]. Magnetic measurements of newly synthesized samples were carried out with the SQUID-magnetometer Quantum Design MPMS-5S. Figure 1 gives the temperature scans of the magnetization for different compounds at the field  $H = 100$  mT. The experimental magnetization curves were used to estimate the ordering temperatures  $T_c$  as the position of the maximums at the derivative  $dM/dT$  (Fig. 1).

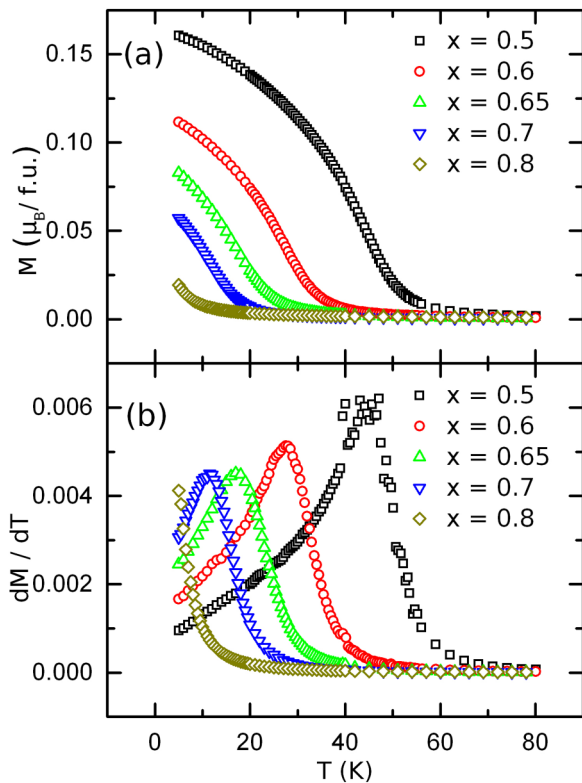


FIG. 1. (Color online) (a) The temperature dependence of the magnetization  $M$  for  $\text{Fe}_{1-x}\text{Co}_x\text{Si}$  compounds with  $x = 0.5 \div 0.8$  at  $H = 100$  mT. (b) The first derivative of the magnetization on the temperature  $dM/dT$ .

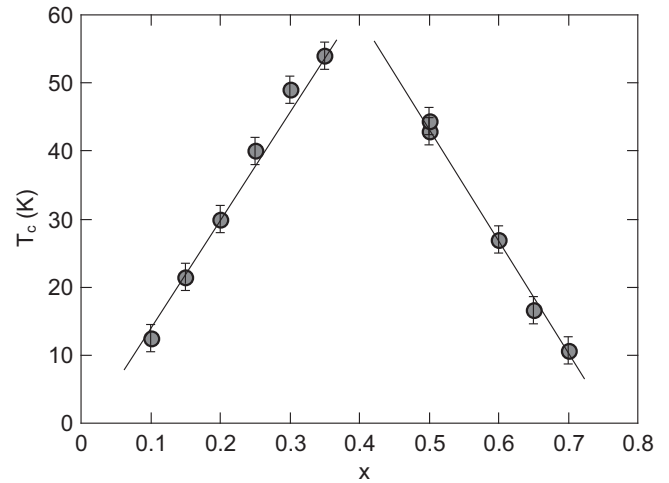


FIG. 2. Dependence of the critical temperature  $T_c$  on the concentration  $x$  of  $\text{Fe}_{1-x}\text{Co}_x\text{Si}$  compounds.

The same analysis has been applied to the SQUID data for the samples studied in Ref. [16] for  $x = 0.1 \div 0.5$ . The  $x$  dependence of the critical temperature  $T_c$  in the range  $x = 0.1 \div 0.7$  is shown in Fig. 2.  $T_c$  increases monotonically on increase of  $x$  from  $0.1 \div 0.4$ . For  $x > 0.4$ ,  $T_c$  decreases again monotonically with  $x$  and approaching 0 at  $x \rightarrow 0.8$ , proving that the compounds under study are magnetically ordered up to  $x = 0.7$ . Notably, the pure compounds do not show any magnetic ordering, while their solid solutions show a remarkable compositional dependence of the ordering temperature. If the exchange interactions is a function of the number of Fe-Co pairs, then for an ideal mixture the maximum of  $T_c$  is expected at  $x = 0.5$ ; the experiment gives  $x = 0.4$  and the reason for the difference is still to be found.

The chirality of the magnetic structure was determined using polarized neutron diffraction [24,25]. We used the protocol similar to one described in Refs. [12,16] for the data analysis. The polarized small-angle neutron scattering (SANS) was carried out at the SANS-1 instrument at the Meier-Leibniz-Zentrum in Garching. The wavelength of the neutron beam was set in the range from 0.6 to 1.2 nm depending on the needed  $Q$  range. A position-sensitive detector with  $128 \times 128$  pixels and a pixel size of 8 mm was used. These settings allowed us to cover a  $Q$  range from  $2 \times 10^{-2}$  to  $1 \text{ nm}^{-1}$ . The initial polarization of the neutron was  $P_0 \approx 0.9$ .

Figure 3 shows the polarized small-angle neutron scattering maps for the compounds MnSi and  $\text{Fe}_{1-x}\text{Co}_x\text{Si}$  with  $x = 0.5, 0.6, \text{ and } 0.7$  at low temperature. For all measurements, the peak width is determined by the particular resolution of the SANS instrument, dominated here by the  $\frac{\Delta\lambda}{\lambda} \approx 10\%$  wavelength contribution. This comes up to a minimal correlation length of  $\approx 600$  nm, resulting in a lower limit for the size of the investigated homochiral helimagnetic domains. As one can see, the MnSi reference sample shows a maximum of the scattering intensity at the right part of the detector with an initial polarization of the neutron beam along the magnetic guide field [Fig. 3(a)]. For  $x = 0.5$  [Fig. 3(b)] and  $x = 0.6$  [Fig. 3(c)] the behavior is similar to the MnSi reference sample and the maximum of the scattering intensity is at

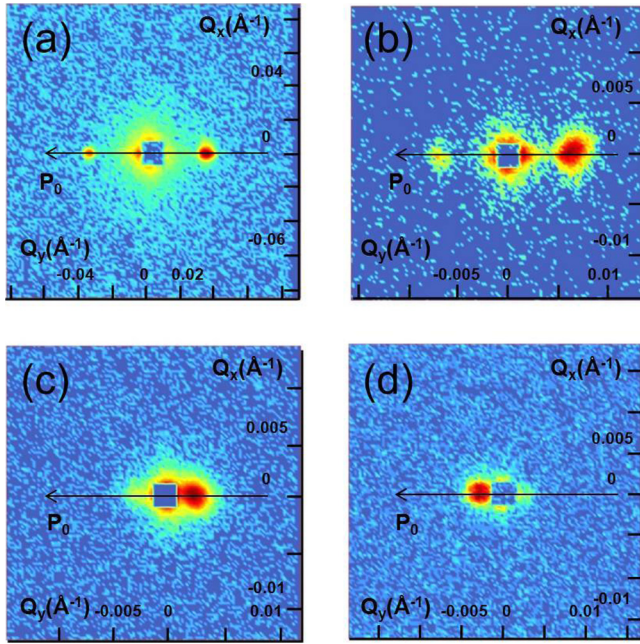


FIG. 3. (Color online) Maps of polarized SANS intensities of MnSi (a) and of  $\text{Fe}_{1-x}\text{Co}_x\text{Si}$  with  $x = 0.5$  (b),  $0.6$  (c), and  $0.7$  (d) for polarization  $+\mathbf{P}_0$  along the guide field at  $T \approx 3.5$  K.

the right side of the scattering maps. In agreement with definitions given previously [16,21], the magnetic chirality for this configuration is  $\gamma_m = -1$ . Clearly, the  $\text{Fe}_{0.3}\text{Co}_{0.7}\text{Si}$  sample shows the opposite behavior [Fig. 3(d)], having  $\gamma_m = +1$ .

The helix wave vector  $|k_s|$  has been extracted from the scattering maps at low temperature ( $T \approx 3.5$  K). Figure 4(a) shows the  $x$  dependence of  $|k_s|$ , the product of the lattice chirality  $\Gamma_c$  and the magnetic chirality  $\gamma_m$  is shown in Fig 4(b). For  $|k_s|$  the value increases from  $|k_s| = 0.121 \text{ nm}^{-1}$  for  $x = 0.1$  to a maximum of  $|k_s| = 0.185 \text{ nm}^{-1}$  for  $x = 0.2$ . For  $x > 0.2$  the value decreases to a minimum  $|k_s| \rightarrow 0 \text{ nm}^{-1}$  at the critical concentration of  $x_c = 0.65$  and increases again to  $|k_s| = 0.026 \text{ nm}^{-1}$  for  $x = 0.7$ . The helix wave vector  $k$  and the Dzyaloshinskii constant  $D$  are linked via the equation

$$k = \frac{SD}{A}, \quad (1)$$

where  $S$  is an average spin per unit cell and  $A$  is the spin wave stiffness [26]. The spin wave stiffness and the spin value are expected to be monotonic functions of the Co content [27,28], and therefore  $|k_s| \rightarrow 0$  implies that  $|D| \rightarrow 0$  at  $x_c$ .

The same concentration  $x_c$  separates two regions with opposite values of the product  $\Gamma_c \times \gamma_m$ , and therefore  $D$  not only goes through zero at  $x_c$  but also changes its sign.

To summarize, we show that the chiral magneto-lattice coupling mapped phenomenologically as the DMI could be applied to control magnetic chirality as needed for yet illusive spintronics applications.

The sign of the Dzyaloshinskii constant  $D$  defines the chirality of magnetic helix relative the structural chirality. The product  $\text{sgn}(D) \times \Gamma_c \times \gamma_m$  is an invariant with respect to inversion and time-reversal operations ensuring that left-handed

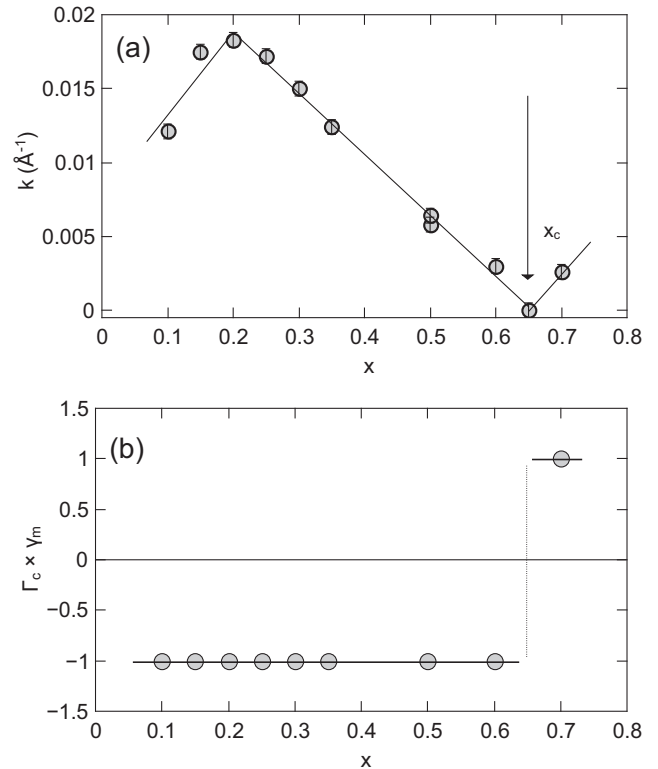


FIG. 4. Dependence of (a) the helix wave vector  $k$  and (b) the product of structural and magnetic chiralities  $\Gamma_c \times \gamma_m$  on the concentration  $x$ .  $x_c$  shows where  $k$  goes to zero.

and right-handed polymorphs have the same energy. The sign of  $D$  depends on  $3d$  element occupying the metal site in  $\text{Fe}_{1-x}\text{Co}_x\text{Si}$ , and also in monogermanides [12,14,15].

Recently, it was shown to be possible to theoretically reproduce the observed change of  $D$  in the similar system  $\text{Mn}_{1-x}\text{Fe}_x\text{Ge}$  [29,30]. Koretsune *et al.* [29] used *ab initio* density-functional theory calculations to compute the spin susceptibility that is directly proportional to the DM interaction. They used a rigid band approximation starting from the electronic structure of  $\text{FeGe}$  as well as  $\text{MnGe}$ . Based on both cases they have been able to qualitative reproduce the observed change of the sign of  $D$  in  $\text{Mn}_{1-x}\text{Fe}_x\text{Ge}$  with concentration  $x$  with  $D < 0$  in the  $\text{FeGe}$  region and  $D > 0$  in the  $\text{MnGe}$  region. It should be noted that the calculated critical concentration deviates somewhat from the measured one  $x_c \approx 0.75$ . Gayles *et al.* [30] have chosen two similar approaches. Their first method is based on an expression for the DMI taken from the Berry phase in the weak spin orbit interaction (SOI) limit, while the second is based on the evaluating the linear slope of the dispersion energy of the long-wavelength flat spin-spiral solutions when including the SOI within first-order perturbation theory. With both methods they have been able to reproduce the change of the sign of  $D$ . They determined the critical concentration at which the sign change take place as  $x_c = 0.8$ , which is in an excellent agreement with the experimental results of  $x_c \approx 0.75$  [12,14]. Furthermore, they developed a minimal tight-binding model which allows them to identify the main mechanism behind the behavior of  $D$ . The responsible mechanism is the dynamics

of the  $d_{x^2-y^2}$ -like states. With increasing  $x$  (change of carrier density)  $d_{x^2-y^2}$  states move from above the Fermi level to below the Fermi level, become occupied, and enter the  $d_{xy}$  states with an opposite spin. Very likely, the observed change of the sign of  $D$  in  $\text{Fe}_{1-x}\text{Co}_x\text{Si}$  is based on a similar mechanism.

The difference in the critical concentrations,  $x_c = 0.65$  for monosilicide and  $x_c = 0.6$  for monogermanides [15], is rather small; more detailed sampling near the critical concentration has to be done to find whether this difference is

significant. Those findings together with the complex nature of the transformation of the helical magnetic structure to a ferromagnetic-like at  $x \rightarrow x_c$  should be subject of further theoretical and experimental studies.

The work was supported by the Russian Foundation for Basic Research (Grants No. 13-02-01468 and No. 14-22-01073) and the Ministry of Education and Science of the Russian Federation, Subsidy No. 14.616.21.0004.

- 
- [1] S. V. Maleyev, *Phys. Rev. Lett.* **75**, 4682 (1995).
- [2] N. M. Chubova, V. A. Dyadkin, E. V. Moskvina, and S. V. Grigoriev, *J. Surf. Invest.: X-ray, Synchrotron Neutron Tech.* **8**, 1020 (2014).
- [3] J. Sinova and I. Zutic, *Nat. Mater.* **11**, 368 (2012).
- [4] R. Naaman, *J. Phys. Chem. Lett.* **3**, 2178 (2012).
- [5] M. Mochizuki, X. Z. Yu, S. Seki, N. Kanazawa, W. Koshibae, J. Zang, M. Mostovoy, Y. Tokura, and N. Nagaosa, *Nat. Mater.* **13**, 241 (2014).
- [6] I. E. Dzyaloshinskii, *Zh. Eksp. Teor. Fiz.* **46**, 1420 (1964) [*Sov. Phys. JETP* **19**, 960 (1964)].
- [7] P. Bak and M. H. Jensen, *J. Phys. C* **13**, L881 (1980).
- [8] O. Nakanishi, A. Yanase, A. Hasegawa, and M. Kataoka, *Solid State Commun.* **35**, 995 (1980).
- [9] V. A. Dyadkin, S. V. Grigoriev, D. Menzel, D. Chernyshov, V. Dmitriev, J. Schoenes, S. V. Maleyev, E. V. Moskvina, and H. Eckerlebe, *Phys. Rev. B* **84**, 014435 (2011).
- [10] S. V. Grigoriev, D. Chernyshov, V. A. Dyadkin, V. Dmitriev, E. V. Moskvina, D. Lamago, Th. Wolf, D. Menzel, J. Schoenes, S. V. Maleyev, and H. Eckerlebe, *Phys. Rev. B* **81**, 012408 (2010).
- [11] D. Morikawa, K. Shibata, N. Kanazawa, X. Z. Yu, and Y. Tokura, *Phys. Rev. B* **88**, 024408 (2013).
- [12] S. V. Grigoriev, N. M. Potapova, S.-A. Siegfried, V. A. Dyadkin, E. V. Moskvina, V. Dmitriev, D. Menzel, C. D. Dewhurst, D. Chernyshov, R. A. Sadykov, L. N. Fomicheva, and A. V. Tsvyashchenko, *Phys. Rev. Lett.* **110**, 207201 (2013).
- [13] V. Dmitriev, D. Chernyshov, S. Grigoriev, and V. Dyadkin, *J. Phys.: Condens. Matter* **24**, 366005 (2012).
- [14] K. Shibata, X. Z. Yu, T. Hara, D. Morikawa, N. Kanazawa, K. Kimoto, S. Ishiwata, Y. Matsui, and Y. Tokura, *Nat. Nanotechnol.* **8**, 723 (2013).
- [15] S. V. Grigoriev, S.-A. Siegfried, E. V. Altynbayev, N. M. Potapova, V. A. Dyadkin, E. V. Moskvina, D. Menzel, A. Heinemann, S. N. Axenov, L. N. Fomicheva, and A. V. Tsvyashchenko, *Phys. Rev. B* **90**, 174414 (2014).
- [16] S. V. Grigoriev, D. Chernyshov, V. A. Dyadkin, V. Dmitriev, S. V. Maleyev, E. V. Moskvina, D. Menzel, J. Schoenes, and H. Eckerlebe, *Phys. Rev. Lett.* **102**, 037204 (2009).
- [17] H. D. Flack, *Acta Crystallogr. Sect. A* **39**, 876 (1983).
- [18] H. D. Flack, *Acta Crystallogr. Sect. A* **55**, 908 (1983).
- [19] *Agilent Technologies*, CrysAlisPro software system. Oxford(UK): Agilent Technologies UK Ltd. (2013).
- [20] G. M. Seldrick, *Acta Crystallogr. A* **46**, 467 (1990).
- [21] M. Tanaka, H. Takayoshi, M. Ishida, Ya. Endoh, *J. Phys. Soc. J.* **54**, 2970 (1985).
- [22] J. Beille, J. Voiron, and M. Roth, *Solid State Commun.* **47**, 399 (1983).
- [23] J. Beille, J. Voiron, F. Towfiq, M. Roth, and Z. Y. Zhang, *J. Phys. F: Met. Phys.* **11**, 2153 (1981).
- [24] S. V. Maleyev, V. G. Bar'yahtar, and R. A. Suris, *Fiz. Tverd. Tela (S.-Peterburg)* **4**, 3461 (1962) [*Sov. Phys. Solid State* **4**, 2533 (1962)].
- [25] M. Blume, *Phys. Rev.* **130**, 1670 (1963).
- [26] S. V. Maleyev, *Phys. Rev. B* **73**, 174402 (2006).
- [27] S. V. Grigoriev, S. V. Maleyev, V. A. Dyadkin, D. Menzel, J. Schoenes, and H. Eckerlebe, *Phys. Rev. B* **76**, 092407 (2007).
- [28] N. Manyala, Y. Sidis, J. F. DiTusa, G. Aeppli, D. P. Young, and Z. Fisk, *Nature* **404**, 581 (2000).
- [29] T. Koretsune, N. Nagaosa, and R. Arita, [arXiv:1503.03777v1](https://arxiv.org/abs/1503.03777v1) [cond-mat.mtrl-sci] (unpublished).
- [30] J. Gayles, F. Freimuth, T. Schena, G. Lani, P. Mavropoulos, R. Duine, S. Blügel, J. Sinova, and Y. Mokrousov, [arXiv:1503.04842v1](https://arxiv.org/abs/1503.04842v1) [cond-mat.mtrl-sci] (unpublished).